D31

N79-24032

AREA SCALING INVESTIGATIONS OF CHARGING PHENOMENA

Paul R. Aron and John V. Staskus
NASA Lewis Research Center

SUMMARY

The charging and discharging behavior of square, planar samples of silvered, fluorinated ethylene-propylene (FEP) Teflon thermal control tape was measured. The equilibrium voltage profiles scaled with the width of the sample. A wide range of discharge pulse characteristics was observed, and the area dependences of the peak current, charge, and pulse widths are described. The observed scaling of the peak currents with area was weaker than that previously reported. The discharge parameters were observed to depend strongly on the grounding impedance and the beam voltage. Preliminary results suggest that measuring only the return-current-pulse characteristics is not adequate to describe the spacecraft discharging behavior of this material. The seams between strips of tape appear to play a fundamental role in determining the discharging behavior. An approximate propagation velocity for the charge cleanoff was extracted from the data. The samples - 232, 1265, and 5058 square centimeters in area - were exposed at ambient temperature to a 1- to 2-nA/cm^2 electron beam at energies of 10, 15, and 20 kilovolts in a 19-meter-long by 4.6-meter-diameter simulation facility at the Lewis Research Center.

INTRODUCTION

It has been clear from the beginning of the spacecraft charging investigation that an understanding of the geometric scaling laws that describe charging phenomena is of fundamental importance. Larger systems are being built, and even larger ones are being seriously proposed for future missions. Worse-case calculations and extrapolations from existing data have a limited reliability and utility. Therefore, experimental studies must be undertaken with larger areas of engineering material than previously tested. There is also an inadequate theoretical understanding of the discharge process. An experimental study of the variation with area of the parameters that describe the discharge process should provide important clues to guide the mathematical modeling effort. Some significant experimental measurements of area effects have been reported in the literature (refs. 1 and 2). Balmain (ref. 1) has systematically investigated area effects in a variety of spacecraft materials. His work was confined to areas of less than 100 square centimeters, but it did give the first clear experimental observation of the scaling of discharge pulse characteristics with area. Bogus (ref. 2) has also reported measurements of area scaling for large samples (3800 cm^2); however, his work has been confined to solar arrays.

At Lewis, an effort has begun to study systematically the area and geometry dependence of the charging and discharging parameters for a variety of spacecraft materials. Because of previous experience with silvered-Teflon thermal control tape, it was chosen as the first material to be tested in this investigation. The large size of the Lewis simulation facility has made it possible to study Teflon samples that are more than an order of magnitude larger than those previously reported.

MATERIALS, APPARATUS, AND PROCEDURE

Materials

The samples consisted of strips of 5-centimeter-wide, silvered, fluorinated ethylene-propylene (FEP) Teflon thermal control tape. The tape is a composite that consists of a 0.011-centimeter-thick sheet of Teflon with, first, a layer of vapor-deposited silver and, second, a layer of vapor-deposited Inconel 600. These layers were followed by a third, a 0.03-millimeter-thick layer of conductive adhesive. The adhesive was two parts GE SR525 silicone rubber mixed with one part silver powder (by weight). The tape was applied to a clean 0.313-centimeter-thick, square aluminum plate in strips extending the full length of the plate. The strips were butted edge to edge. The edges and the back of the plate were not covered. However, no part of the bare plate was exposed to the direct electron beam. The tape was applied with finger pressure and was tested in vacuum to have a resistance from the silver layer to the plate of approximately 60 ohms for a 1-square-centimeter area. Three sample assemblies were prepared - with areas of 232, 1265, and 5058 square centimeters.

Apparatus

Figure 1 shows the interior of the vacuum tank and the experimental arrangement. The 1265-square-centimeter sample is shown in place. It is fixed to the sample carriage, a vertical bar that can be moved remotely up to 1.1 meters horizontally, perpendicular to the tank axis. To the right of the sample is a stainless-steel beam shield. Behind the sample and, therefore, not visible in the figure is a 10-square-centimeter Faraday cup. Below and to the left of the sample is the arm on which are fixed the heads of two TREK model 340 HV electrostatic voltmeters. The spacing between the heads is adjustable and they are swept in a vertical arc across the sample surface. The probes were typically spaced 2 millimeters from the sample.

The sample assembly was grounded in one of two ways. In the first configuration, which is referred to as the 50-ohm configuration, the aluminum plate was insulated from the carriage and the tank structure. A 50-ohm coaxial lead approximately 10 meters long was brought from the sample out through the tank wall. The shield was grounded at the tank wall. The center conductor passed through the core of a Pearson model 110 current transformer. The lead was then brought to a switch that could ground it through a 50-ohm resistor or apply it to the input of an electrometer. This configuration is shown in figure 2 as a solid line. In the second configuration, which is referred to as the low-impedance configuration, the insulator between the sample and the carriage was replaced by an 8-centimeter-long aluminum post threading the core of the Pearson current transformer. This configuration is shown in figure 2 as the dashed line. It was conceived to minimize the sample impedance to ground.

The current transformer is useful for signals with rise times greater than 50 nanoseconds. The transformer output was monitored with both a Tectronix model 7834 storage oscilloscope and a Biomation model 8100 waveform recorder. The waveform recorder was used in the pretrigger mode. In this mode it stores the output voltage of the Pearson transformer as a function of time over a selected interval (usually 20 μsec). This time interval includes a selectable time interval before the trigger. This capability is particularly useful for transient phenomenon as it eliminates the question about what happened before the trigger point. The signal was played back slowly through an integrator, and it and its time integral were recorded on a two-channel strip-chart recorder.

The output of the electrostatic voltmeters and their time integrals were recorded along with the various electrometer currents, position readouts, etc., on a multichannel strip-chart recorder. The electron flux (1 to 2 nA/cm^2) was generated by two Lewis electron guns (ref. 3). The guns were mounted next to one another, on either side of the tank axis, approximately 10 meters from the sample plane. The current distribution in this plane was measured by an array of current collection disks. The flux varied ±30 percent over the largest sample area. The electron trajectories were minimally affected by the Earth's magnetic field since the mild steel in the outer wall of the vacuum tank reduced the field by about a factor of 10.

A loop antenna feeding a three-level radiofrequency transient-event counter was located near the sample and served to count discharges and sort them by amplitude. Also located near the sample and visible in figure 1 in the upper right corner was a gaseous-nitrogen plasma source that was used to neutralize the surface charge on the sample.

The vacuum tank is a horizontal steel cylinder 19 meters long and 4.6 meters in diameter pumped by 20 liquid-nitrogen-baffled 91-centimeter-diameter oil diffusion pumps. It was comfortably operated at approximately 2.7×10^{-8} N/m^2 (2×10^{-6} torr) for these tests and has a no-load pressure of approximately 1.3×10^{-9} N/m^2 (10^{-7} torr).

Test Procedure

In the 50-ohm configuration the samples were exposed sequentially to 10-, 15-, and 20-kilovolt beams. The imbedded charge was neutralized with the plasma source between exposures. The sample was irradiated at each voltage for a short time (15 to 60 sec), and the surface voltage profiles were measured over the entire sample area at the end of each interval. At 10-kilovolt exposure the three samples were charged to equilibrium (fig. 3) with the sample ground completed through the electrometer (fig. 2). At 15- and 20-kilovolt exposures the samples did not charge to equilibrium but began exhibiting breakdowns when the maximum surface voltage was as low as 8.5 kilovolts. With the ground switched from the electrometer to the 50-ohm termination, the return-current pulses were recorded until a representative group had been assembled. As the last procedure in the run, the electron beam was turned off just before the next predicted breakdown and the surface voltage profiles were measured. The beam was then turned back on until the next discharge and then immediately turned off and the surface resurveyed. These data give the total charge on the surface before and after a discharge.

After this sequence of measurements was made for the three samples, they were remounted in the low-impedance configuration, and their discharge behavior was remeasured at both 15- and 20-kilovolt electron fluxes.

RESULTS

Charging

Figure 3 is a typical time history of the charge buildup on a 232-square-centimeter sample in a 10-kilovolt electron beam. The voltage profiles were taken with the probes passing across approximately the middle of the sample. The individual strips of tape are revealed by the sharp dips on the surface voltage at the seams, where the tape strips are butted.

During the initial stages of charging, the distribution of charge on the surface should mirror the actual flux distribution (assuming, of course, that the surface properties are uniform over the sample). The observed variation of the surface voltage with the position of the 232- and 1265-square-centimeter samples is consistent with the measured ±30 percent variation of the beam flux over the sample plane. The largest sample (5058 cm^2) shows a somewhat wider variation, the origin of which is undetermined. All three samples at equilibrium exhibit a uniform profile except for the gaps and a characteristic falloff at the edges.

The equilibrium voltages at the center were 8.0, 7.2, and 7.6 kilovolts for the 232-, 1265-, and 5058-square-centimeter samples, respectively. The voltage profiles at equilibrium, in all three cases, do not exhibit complete bilateral symmetry. All are skewed in the same way, suggesting a lack of symmetry in the experimental arrangement as the cause.

Figure 4 shows the normalized voltage profiles, where the distance x is scaled by the half-width w of the sample and the voltage V by the maximum voltage V_m. In these reduced coordinates the three samples are, to first order, identical if the seams are ignored. This observed scaling with sample width is inconsistent with the model proposed by Parks and Mandell (September 1976 Monthly Progress Report on NASA Contract NAS3-20119, Systems, Science, and Software) and used by Stevens, et al. (ref. 4) to fit their edge-gradient data. Their model considers surface and bulk resistance along with a one-dimensional current-balance description (ref. 5) to predict the edge profiles. The inability of the Parks-Mandell model to predict something as fundamental as the observed scaling indicates that the dominant physical mechanism that controls the edge profile has not been incorporated. Multidimensional effects are the most obvious possibilities. In particular, the spreading of the beam due to the finite width of the sample should be considered. The deflection of the incoming particles will certainly be greater for larger samples.

Discharging

Discharge phenomenon in these samples were studied at beam voltages of 15 and 20 kilovolts. Discharging seemed to begin when the maximum sample voltage was as low as 8.5 kilovolts. These early discharges were characterized by their small size relative to the more typical breakdowns. Figure 5 is a time history of the breakdown behavior of the 232-square-centimeter sample, which is typical. The voltage profiles were taken acros approximately the center of the sample and transverse to the tape direction.

The seams are apparent in figure 5(a) as two small dips. The probe sweeps over a 4-kilovolt calibration bar at the end of its travel. Figure 5(a) shows the profile after 215 seconds of charging with a 15-kilovolt electron beam. Figure 5(b) shows the same profile just after the first breakdown and 270 seconds after the start of charging. The breakdown is evident as a charge-depleted region around the left tape seam. The extent of this charge-depleted region along the seam direction is shown in figure 6. The only two sweeps that show depletion are figures 6(c) and (d), demonstrating that the length of the depleted region is no more than 768 centimeters long and is away from the ends of the sample. Figure 5(c) shows the profile after further charging; no breakdowns were observed on the arc counter or the current monitors. The overall voltage level is higher than in figure 5(b) and the charge-depleted region is filling in. Figure 5(d) shows the profile taken after 370 seconds of charging and immediately after the second observed breakdown. This profile, when compared with figure 5(c), indicates that both seams broke down. Figure 5(e) shows the same profile after 600 seconds of charging and before the next breakdown which occurred at 665 seconds. The results of that breakdown are shown in figure 5(f). Before this breakdown, the maximum surface voltage increased over that in figures 5(c) and (d) and almost total charge cleanoff resulted. Almost total charge cleanoff is typical of the behavior of this size sample for most of the subsequent breakdowns.

Qualitatively, the preceding sequence of events is analogous to the behavior seen commonly on high-voltage insulators when they are initially brought up to their working voltage. In this case, gaps that before breakdown have the largest voltage gradients (electric fields) break down initially at low voltages and, by depleting the charge near them, reduce the locally high electric field. The regions away from the gaps can then charge to even higher voltage until the next most sensitive high-electric-field-region breaks down. This allows the sample voltage to go even higher. This process continues until there are many sites similarly sensitive and quasi-repetitive behavior sets in.

Figure 7 shows three examples of the more typical return-current pulses I resulting from the discharge of the 232-square-centimeter sample. Figures 7(a) and (b) show data taken with the 50-ohm grounding configuration at 15 and 20 kilovolts, respectively. Figure 7(c) shows a typical pulse with the low-impedance grounding configuration. The vertical gain is a factor of 2 smaller than in figures 7(a) and (b). A most distinctive characteristic of this sample when tested in the low-impedance configuration is the appearance of a positive precursor. That is, there is an initial downward spike that represents a positive current leaving the sample. Here, and in all the return-current-pulse data shown, a signal greater than zero represents a current of negative charge leaving the surface (ref. 6). Only this sample, in this configuration, exhibited a positive precurser and it always did. However, the net charge leaving the surface was always negative, as in the other samples. This positive precurser may be related to the positive charge bursts reported by Yadlowsky (ref. 7). He observed both positive and negative charge bursts with different time evolutions in breakdowns in bulk Teflon. This would suggest that such currents of both positive and negative particles are contributing to give the result reported here.

Figure 8 shows some typical return-current pulses from the 1265-square-centimeter sample. They have been chosen to demonstrate the range of sizes and shapes observed. The nonrepeatability of the shape, the wide variety of sizes, and the general lumpy quality of the pulses suggests that they are composites of many small breakdowns. The low-impedance pulses (figs. 8(c), (d), and (e)), though similar in overall shape, have higher frequency noise components than the 50-ohm pulses. Figure 9 shows some pulses from the 5058-square-centimeter sample. The same comments concerning the variability of size and shape that were made about the 1265-square-centimeter sample are appropriate here.

For the purpose of discussing area effects the individual return-current pulses are described by three parameters: the maximum current I, the total charge Q, and the time Δt, where Δt is defined as the width of the pulse at $I/2$. Except for the first few discharges that were described earlier, there was no evident systematic dependence of these parameters on the discharge history. A distribution function for these parameters was constructed by choosing a narrow interval of the variable and plotting the fractional number of events occurring in the interval. A smooth curve was then drawn through the point.

Figure 10 is an example of such a distribution function for the peak value I of the return-current pulses observed with the 1265-square-centimeter sample at 20 kilovolts with the low-impedance grounding configuration. The horizontal bar indicates the current interval.

These distributions were characterized by three parameters: the largest value of the parameter observed, denoted by the subscript M; the value of the parameter at the peak of the distribution function, which can be thought of as the most probable value, denoted by the subscript MP; and, finally, the width Δ of the distribution function at 1/2 the MP value. Table I contains the reduced data arranged by area, beam voltage, and grounding configuration. The last two columns give the total number N_T of discharge pulses recorded and analyzed for both grounding configurations. The small number of pulses studied in the low-impedance, 15-kilovolt, 232-square-centimeter case resulted from a reluctance of the sample to break down under these conditions.

Figure 11 shows the data for the maximum current I_M observed as a function of area for the two grounding configurations and beam voltages. It was expected that the area dependence of this current would be of interest because it is a worst-case parameter. Where it seemed appropriate, a least-squares fit was drawn through the three points. The 20-kilovolt, 50-ohm data fit an $I_M = 14.3\ (A)^{0.25}$ line, where A denotes area. The low-impedance data at either beam voltage does not lend itself to a single-term power-law description, and straight lines are used to connect the points. The area scaling exhibited by the 20-kilovolt, 50-ohm data is weaker than the $(A)^{0.575}$ reported by Balmain (ref. 1) for smaller samples. It is difficult, however, to compare his work directly with that reported here since his grounding was different, his statistical treatment of the data was not the same, and his current density was three orders of magnitude larger. However, his data do extrapolate in close agreement with the low-impedance, 20-kilovolt, 232-square-centimeter point.

Two qualitative observations should be made about the maximum-current data in figure 11. First, in agreement with A. Rosén of TRW (private communication), the grounding configuration had a significant effect on the behavior. For example, at 20 kilovolts significantly larger currents were observed with the low-impedance ground than with the 50-ohm ground. However, 15 kilovolts the opposite is true. Second, both the 50-ohm and low-impedance data exhibit a weaker area dependence with a 15-kilovolt beam than with a 20-kilovolt beam.

Figure 12 shows the most probable peak current I_{MP} as a function of sample area in the same format as in the previous figure. The same strong dependence of the behavior of this parameter at 15 kilovolts on the nature of the grounding is observed. At 20 kilovolts the area dependence of I_{MP} is clearly much weaker than that exhibited by I_M. In fact, it would seem that to a first approximation, I_{MP} is independent of the area.

Figure 13 shows the maximum charge Q_M in the same format as in the two previous figures. At 20 kilovolts both grounding configurations show good least-squares fits to $Q_M = K(A)^{0.78}$, where K is a constant. The low-impedance configuration gave a somewhat larger value of K (0.38) than the 50-ohm configuration (0.30). The 15-kilovolt, 50-ohm data (fig. 13(b)) are fit (rather poorly) by $Q_M = 0.75\ (A)^{0.65}$, which is weaker than the 20-kilovolt scaling. But, given the quality of the fit, no conclusion can be drawn concerning the beam-voltage dependence of the exponent.

Figure 14 shows the most probable charge Q_{MP} as a function of area. At 20 kilovolts the dependence of this parameter on area is significantly weaker than that of Q_M, but at 15 kilovolts its behavior is similar to that of its Q_M counterpart. Both the Q_M and Q_{MP} data show the same sensitivity to the grounding configuration as does I_M in that, at 20 kilovolts, a low-impedance ground increases the charge over the 50-ohm value but at 15 kilovolts it decreases it.

Figure 15 shows the maximum discharge time Δt_M as a function of area. All four sets of data fit $\Delta t_M = K(A)^x$ very well. The values of K and x for the four cases are given on the figure. The 50-ohm data for both voltages show that Δt_M scales approximately as the first power of the area, but the low-impedance data exhibit significantly weaker scaling.

Figure 16 shows the data for the most probable discharge time Δt_{MP}. The 20-kilovolt data in both grounding configurations fit $\Delta t_{MP} = K(A)^x$ in a convincing way, but with values of x significantly smaller than in the Δt_M cases. It appears that Δt_{MP} scales approximately as the square root of the area. This dependence suggests that a characteristic linear dimension may control the breakdown behavior. If it is assumed that the most probably breakdown starts somewhere in a seam, propagates along it at constant velocity, and is limited by the length of a single seam, the coefficient K can be interpreted as $1/2fv$, where v is the propagation velocity. The factor 2 is approximate and is inserted because the most probable pulse would start somewhere near the middle and propagate in both directions, f is a correction that would convert Δt to the total time the pulse propagates down the gap. A model of the discharge process that could predict the return-current-pulse shape is required to accurately evaluate f. Such a model does not exist, but f is assumed to be near 2. Within the limit of this crude description, the propagation velocity v is approximately 1.5×10^7 cm/sec for the 50-ohm data.

Discharge Phenomenology

A consideration of the basic physics of the discharge process in the geometry being studied here immediately calls to question the meaning of the pulse-current measurements described in this paper. Figure 17 schematically describes the experimental situation. In the figure, Q_{before} and Q_{after} are the net charge in the surface of the sample just before and just after the breakdown, respectively; Q_{pulse} is that part of the charge that goes to the baseplate in such a way as to go through the meter; and Q_{short} is that part of the charge that goes to the baseplate without going through the meter. Two contributions to Q_{short} are shown. The lower one corresponds to charge going around the edge of the sample and the upper one, which may be the largest part, corresponds to charge going down the seam to the baseplate.

There is no way, given the present limited understanding of the breakdown process, to predict the relative sizes of Q_{pulse} and Q_{short}. Their ratio should be governed by the details of the experimental geometry, materials, etc. Further, there is reason to expect that their characteristic time evolutions (Δt, e.g.) would be different since the characteristic impedance of the two paths is not likely to be the same. Since Q_{short} would probably have the lower impedance path, its Δt may be significantly smaller than the Δt corresponding to Q_{pulse}. In this experimental arrangement there is no way to determine directly the current-time signature corresponding to Q_{short}, but its magnitude was determined by applying the charge conservation equation shown in figure 17. Any conclusions drawn from these data must be considered to be tentative since only one pulse for each area and beam voltage was considered and only the 50-ohm grounding configuration was used.

The total charge on the surface before the pulse Q_{before} and the charge after the pulse Q_{after} were determined by integrating the surface voltage profiles over the sample area and from the known ratio of capacitance to area ($0.17\ \mu F/m^2$). The sample was treated as a parallel-plate capacitance with the surface of the Teflon as one plate and the silver the other.

Figure 18 summarizes the data for the three charges - Q_{after}, Q_{pulse}, and Q_{short} - as a function of area for the two beam voltages. The charges are expressed as a fraction of Q_{before}. The data in figure 18(a) demonstrate that almost complete charge cleanoff occurs for the 232-square-centimeter sample, but the larger samples show that there is a tendency to saturation at a Q_{after}/Q_{before} of about 0.3. The fraction in the observed pulse Q_{pulse}/Q_{before} seems to drop from about 0.4 for the smallest area to about 0.3 at the largest area. The fraction in the unobserved pulse Q_{short}/Q_{before} starts at about 0.5 and drops to 0.3 or 0.4 at the largest area. Most importantly, it is certainly of the same order as Q_{pulse}/Q_{before} at all areas studied. This result clearly demonstrates that the experimental characterization of discharge behavior in ground tests such as are described in this paper must be done in a manner that considers the contribution of Q_{short} if results useful for extrapolation to spacecraft behavior are to be obtained.

CONCLUDING REMARKS

The charging and discharging characteristics of large-area samples of silvered Teflon tape presented herein demonstrate a complex behavior. These results are preliminary. There is much work to be done and many avenues to explore before an unambiguous picture can emerge. Even at this stage of the investigation, however, some definite conclusions can be drawn.

The 10-kilovolt charging data demonstrate that the edge-voltage profiles scale with the width of the sample. This implies that the existing one-dimensional model, which invokes bulk and surface currents, is incomplete and that multidimensional effects such as beam spreading must be included in any realistic model of insulator charging.

The discharge pulse data demonstrate that the grounding configuration is of real significance. It modifies both the magnitudes of the discharge parameters and in most cases their apparent scaling with area. The same statement can be made about the effect of beam voltage. This is a clear warning that tests with distributed fluxes and spacecraft-like configurations may be mandatory for a realistic simulation of spacecraft materials discharging behavior.

The first few discharges always take place at seams, in the high-voltage region of the sample. However, the role of seams in typical breakdowns is not completely clear. (This study does not distinguish clearly between seam-length effects and area effects since, for these samples, the seam length scales to a first approximation directly as the area.) This ambiguity can and should be resolved by measurements with solid insulator films.

The charge-balance results demonstrate that measuring only the return-current-pulse characteristics does not adequately define the behavior of these materials for spacecraft applications. Consideration must be given to the magnitude and time evolution of Q_{short}. The time evolution of Q_{short} may not be related in any simple way to the observed time evolution of the return-current pulse.

Although the maximum peak currents continue to increase with area ($I \sim A^{0.4}$), the observation that the most-probable peak currents seem to be nearly independent of area suggests that there may be some limiting sample area that contributes to a pulse. Very large areas may also exhibit peak currents that appear area independent since the highest current pulse may continue to scale, but the probability of a high pulse being observed may decrease.

The discharge propagation velocity of 1.5×10^7 cm/sec extracted from these data could provide a clue to the nature of the dominant physical phenomenon controlling the discharge process.

REFERENCES

1. Balmain, K. G.; Kremer, P. C.; and Cuchanski, M.: Charged Area Effects on Spacecraft Dielectric Arc Discharges. Proceedings of 1978 Symposium on the Effect of the Ionosphere on Space and Terrestrial Systems. Office of Naval Research and Naval Research Laboratory, 1978, Session IV, pages 4-5.

2. Bogus, K. P.. Electrostatic Charging Effects on Deployable Solar Arrays. Presented at the Workshop on Space Technology, (DERTS, Toulouse, France), July 1977.

3. Berkopek, F. D.; Stevens, N. J.; and Sturman, J. C.: The Lewis Research Center Geomagnetic Substorm Simulation Facility. Proceedings of the Spacecraft Charging Technology Conference. C. Pike and R. K. Lovell, eds., AFGL-TR-77-0051 and NASA TM X-73537, 1977, pp. 423-430.

4. Stevens, N. J.; Purvis, C. K.; and Staskus, J. V.: Insulator Edge Voltage Gradient Effects in Spacecraft Charging Phonomena. NASA TM-78988, 1978.

5. Purvis, C. K.; Stevens, N. J.; and Oglebay, J. C.: Charging Characteristics of Materials. Comparison of Experimental Results and Simple Analytical Models. C. Pike and R. K. Lovell, eds., AFGL-77-0051 and NASA TM X-73537, 1977, pp. 459-486.

6. Adams, R. C.; and Nanevicz, J. E.. Spacecraft Charging Studies of Voltage Breakdown Processes on Spacecraft Thermal Control Mirrors. Spacecraft Charging by Magnetospheric Plasmas, A. Rosen, ed. Progress in Astronautics and Aeronautics, vol. 47, 1975, pp. 225-235.

7. Yadlowsky, E. J.; Hazelton, R. C.; and Churchill, R. J.. Puncture Discharges in Surface Dielectrics as Contaminant Sources in Spacecraft Environments. (Colorado State Univ.; NASA Contract NSG-3145.) NASA CR-157105, 1978.

TABLE I. - REDUCED DATA ON INDIVIDUAL RETURN-CURRENT PULSES

Sample area, cm^2	Beam voltage, kV	Grounding configuration[a]																			
		50 Ω	LI	50 Ω	LI	50 Ω	LI	50 Ω	LI	50 Ω	LI	50 Ω	LI	50 Ω	LI	50 Ω	LI	50 Ω	LI	50 Ω	LI
		Maximum current, I_M, A		Most probable current, I_{MP}, A		Most-probable-current interval, ΔI_{MP}, A		Maximum total charge, Q_M, μC		Most probable total charge, Q_{MP}, μC		Most-probable-total-charge interval, ΔQ_{MP}, μC		Maximum discharge time, Δt_M, μsec		Most probable width of pulse at I/2, Δt_{MP}, μsec		Most-probable-width interval, $\Delta(\Delta t_{MP})$, μsec		Total number of discharge pulses recorded and analyzed, N_T	
5058	20	240	330	52	63	125	250	260	340	30	135	130	130	3.6	2.7	1	1	0.7	1	36	25
	15	128	32	108	20	80	25	223	75	155	25	80	65	3.5	4	1.4	1.4	.25	.9	38	16
1265	20	110	138	63	50	50	100	68	80	50	50	65	100	1.1	1.3	.6	.6	.4	.4	16	26
	15	73	45	60	20	40	25	50	65	38	20	25	35	1	2.1	.5	.7	.4	.4	11	25
232	20	62	140	55	135	30	25	23	30	13	30	25	25	.25	.4	.22	.28	.02	.1	12	22
	15	60	23	58	22	2	2	32	7	25	5	10	5	.2	.95	.2	.85	0	.2	10	2

[a]50 Ω denotes 50-ohm grounding configuration (fig. 2); LI denotes low-impedance grounding configuration (fig. 2).

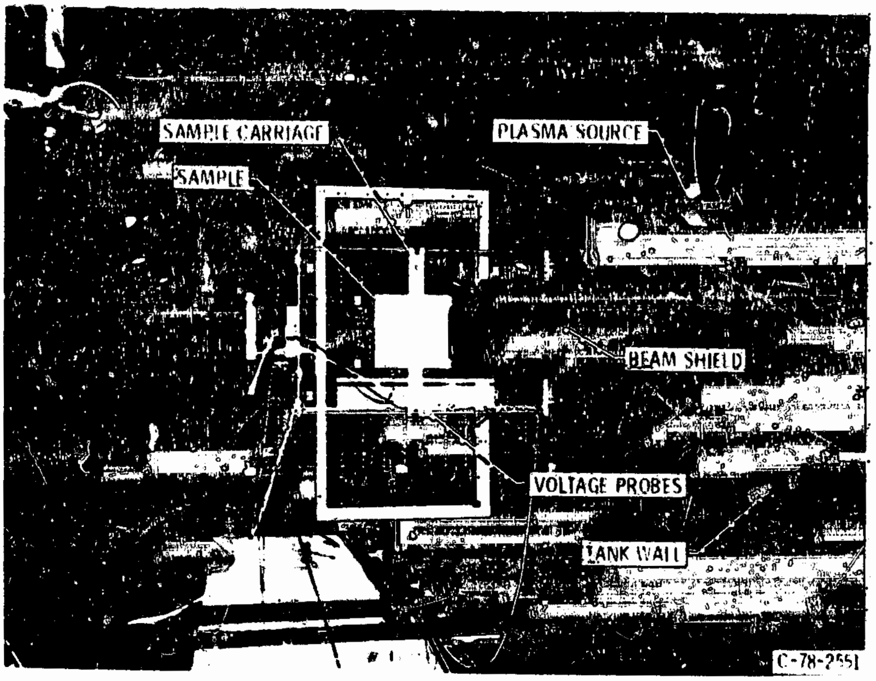

Figure 1. - Vacuum-tank interior and experimental arrangement.

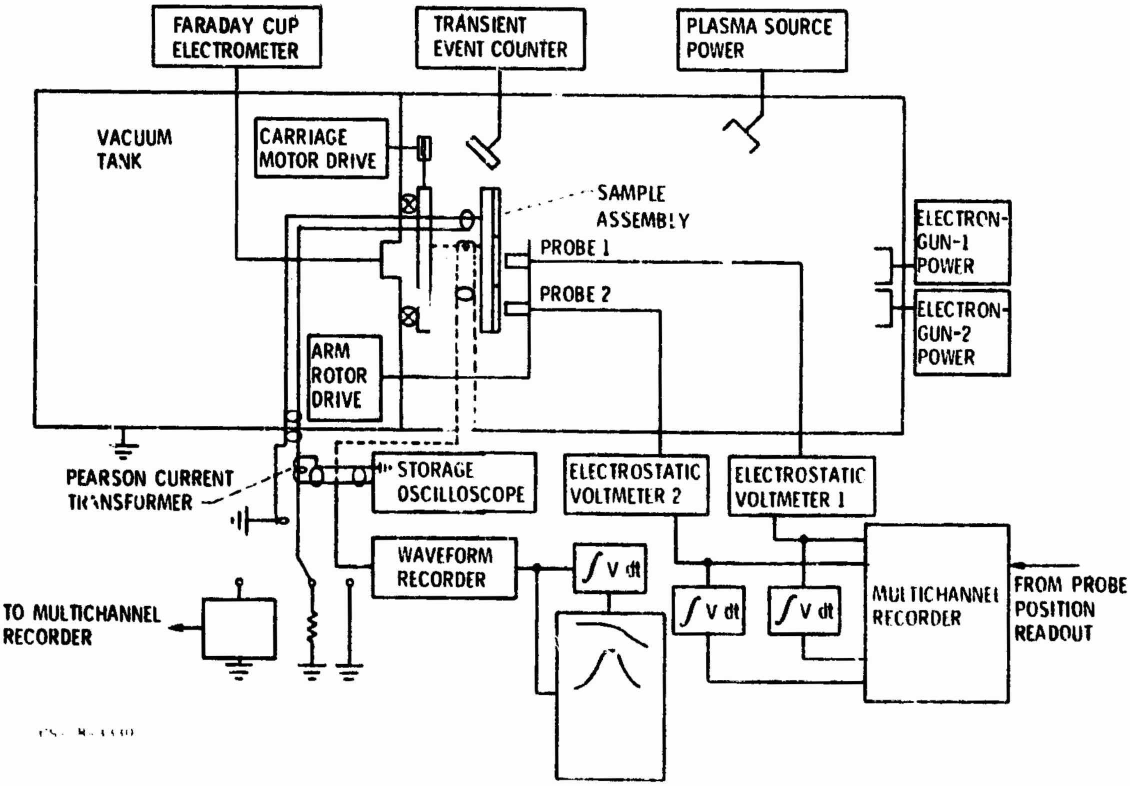

Figure 2. - Area-effects test facility.

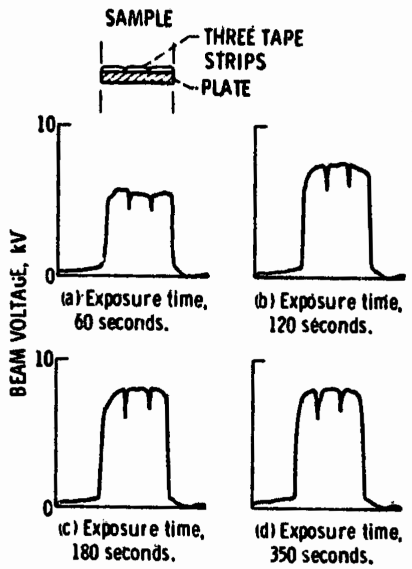

Figure 3. - Voltage profiles for 232-square-centimeter sample and 10-kilovolt beam.

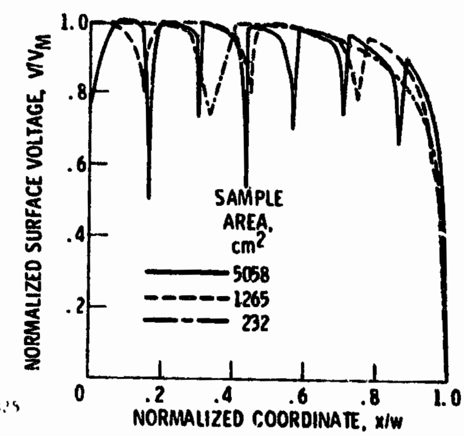

CS-78-3325

Figure 4. - Equilibrium surface-voltage profiles - normalized.

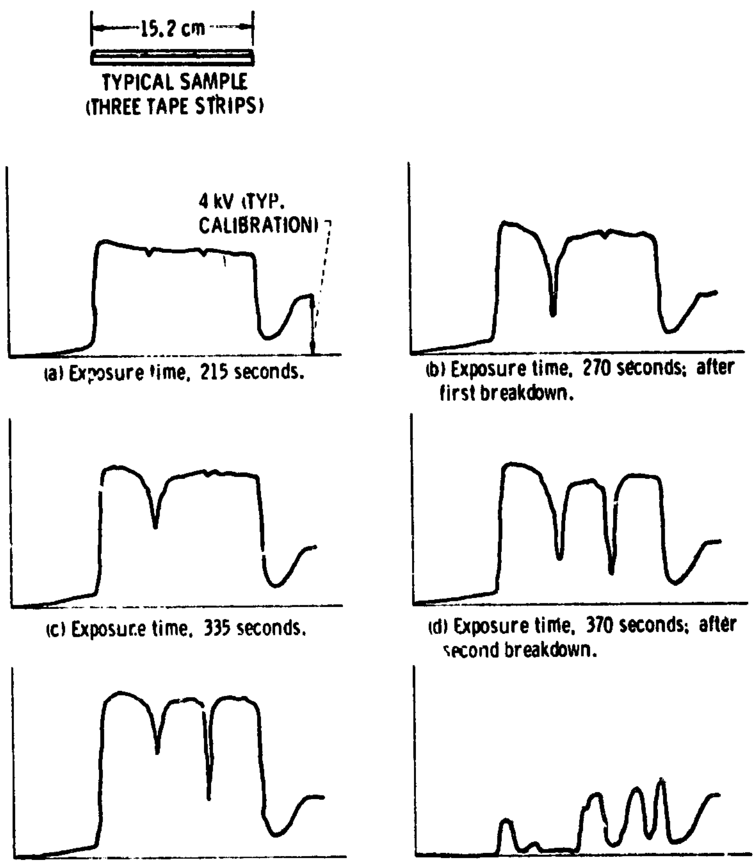

(a) Exposure time, 215 seconds.

(b) Exposure time, 270 seconds; after first breakdown.

(c) Exposure time, 335 seconds.

(d) Exposure time, 370 seconds; after second breakdown.

(e) Exposure time, 600 seconds.

(f) Exposure time, 666 seconds; after third breakdown.

Figure 5. - Center sweeps for 232-square-centimeter sample and 15-kilovolt beam.

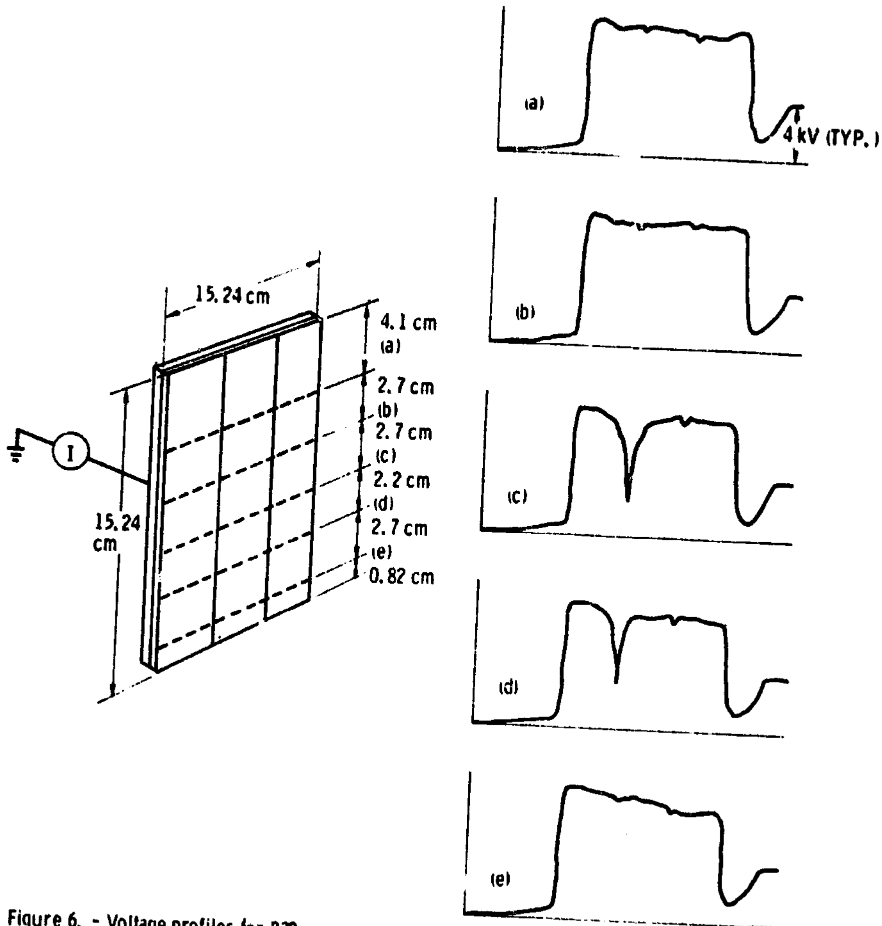

Figure 6. - Voltage profiles for 232-square-centimeter sample at 270 seconds of charging.

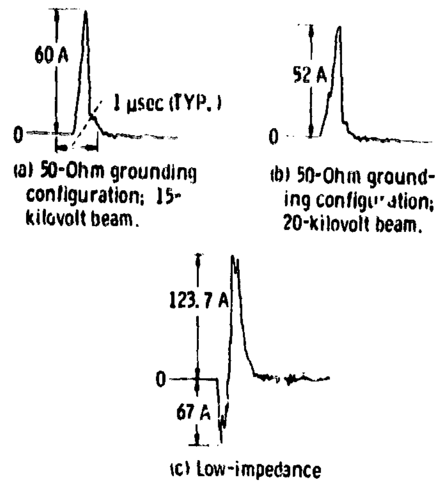

(a) 50-Ohm grounding configuration; 15-kilovolt beam.

(b) 50-Ohm grounding configuration; 20-kilovolt beam.

(c) Low-impedance grounding configuration; 20-kilovolt beam.

Figure 7. - Return-current pulses for 232-square-centimeter sample.

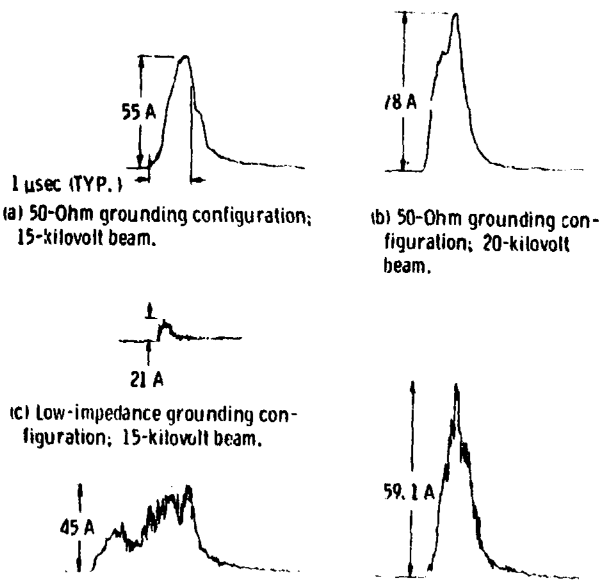

(a) 50-Ohm grounding configuration; 15-kilovolt beam.

(b) 50-Ohm grounding configuration; 20-kilovolt beam.

(c) Low-impedance grounding configuration; 15-kilovolt beam.

(d) Low-impedance grounding configuration; 15-kilovolt beam.

(d) Low-impedance grounding configuration; 20-kilovolt beam.

Figure 8. - Return-current pulses for 1265-square-centimeter sample.

(a) 50-Ohm grounding configuration; 15-kilovolt beam.

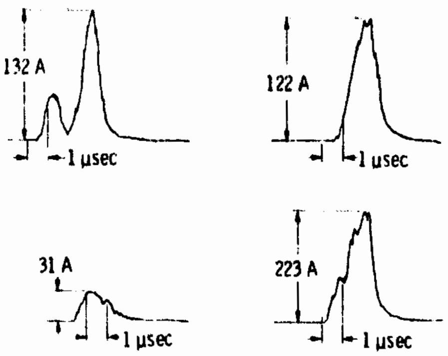

(b) 50-Ohm grounding configuration; 20-kilovolt beam.

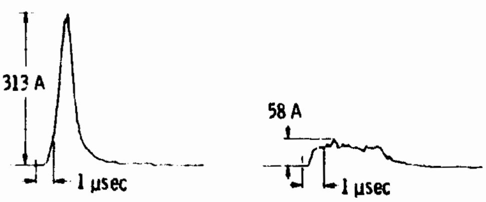

(c) Low-impedance grounding configuration; 20-kilovolt beam.

Figure 9. - Return-current pulses for 5058-square-centimeter sample.

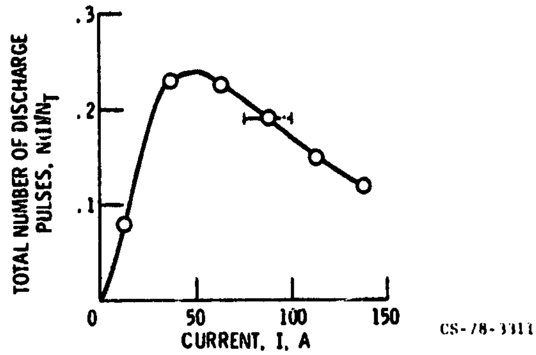

Figure 10. - Current distribution function for 1265-square-centimeter sample in 20-kilovolt beam.

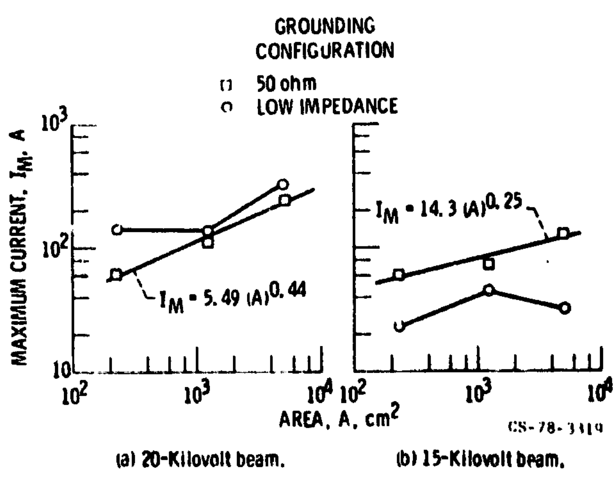

Figure 11. - Maximum return current as function of area.

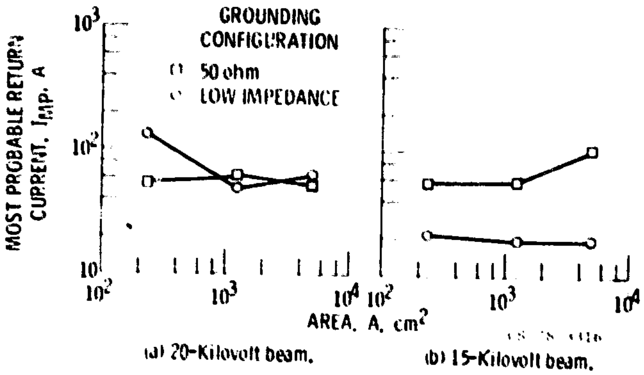

Figure 12. - Most probable return current as function of area.

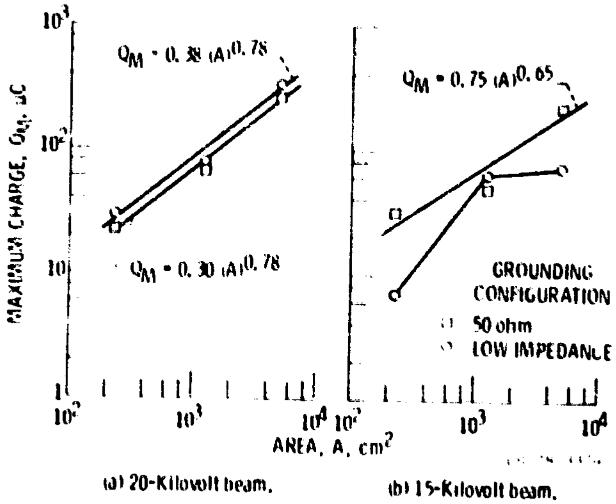

Figure 13. - Maximum charge as function of area.

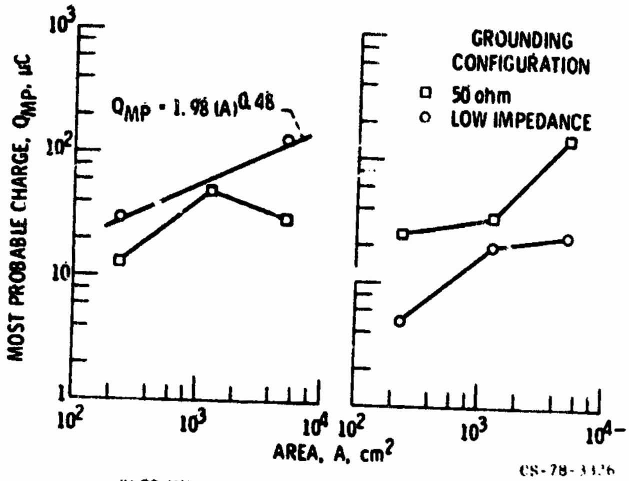

(a) 20-Kilovolt beam.

(b) 15-Kilovolt beam.

Figure 14. - Most probable charge as function of area.

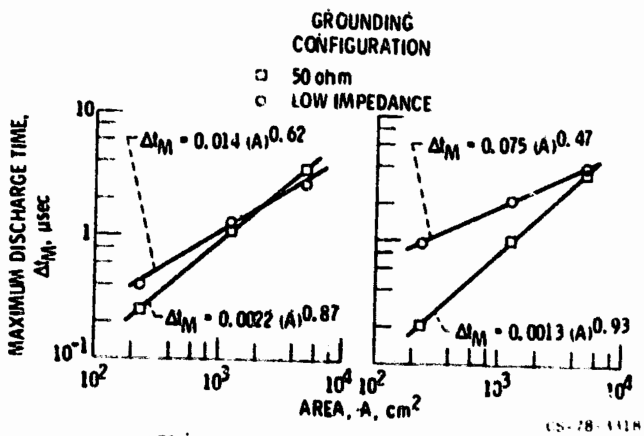

(a) 20-Kilovolt beam.

(b) 15-Kilovolt beam.

Figure 15. - Maximum discharge time as function of area.

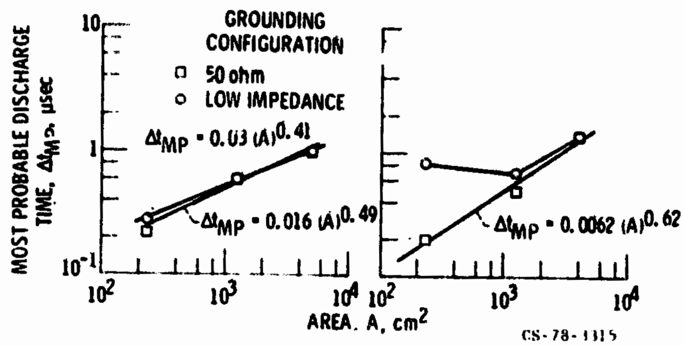

(a) 20-Kilovolt beam. (b) 15-Kilovolt beam.

Figure 16. - Most probable discharge time as function of area.

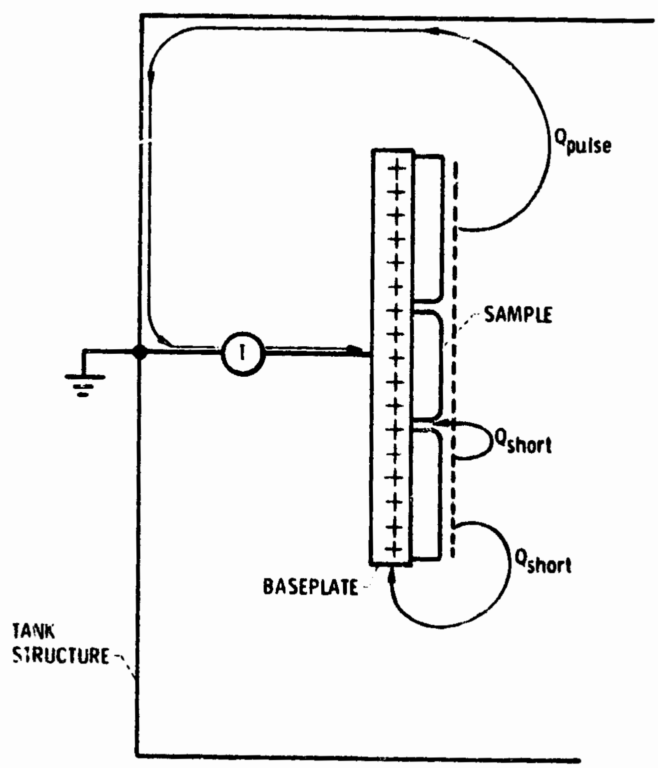

$Q = \int I\, dt$

$Q_{before} = Q_{after} + Q_{pulse} + Q_{short}$

Figure 17. - Breakdown charge distribution.

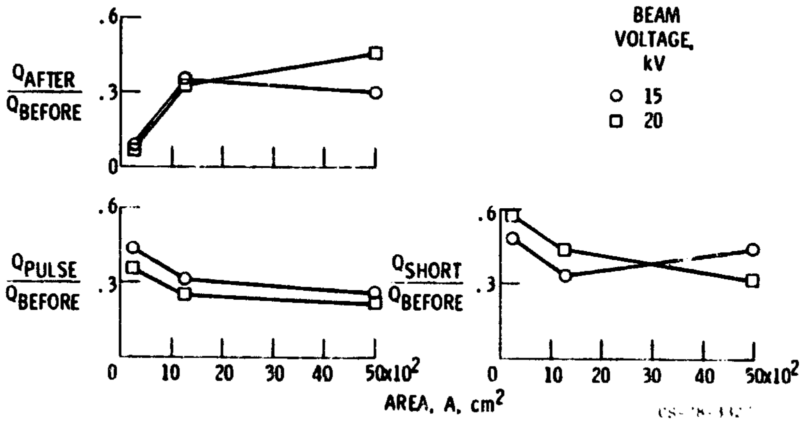

Figure 18. - Postbreakdown charge distribution.